Excitation of electrostatic and whistler waves by a magnetic antenna

G. Yu. Golubyatnikov, S. V. Yegorov, A. V. Kostrov, E. A. Mareev, and Yu. V. Chugunov

Institute of Applied Physics, Academy of Sciences of the USSR

A study is reported of the electrodynamic characteristics of a magnetic antenna in the lower hybrid frequency range in an inhomogeneous magnetoactive plasma. The radiated power is found to exhibit a resonance as a function of the ambient-plasma density. This is due to the presence of a region in which the quasineutrality condition is violated near the surface of the source. The coefficients describing the excitation of electrostatic and whistler waves by a magnetic antenna in an inhomogeneous magnetized plasma are found. The types of wave excited by the source for different parameters of the ambient plasma were identified as a result of the combined measurements of the antenna impedance and the structure of the radiation field. The mode excitation coefficients were also determined in this way, and the results were compared with calculations. The spatial modulation of an electrostatic wave packet has been observed and investigated.

INTRODUCTION

There have been many space and laboratory experiments in recent years in which the emission of electromagnetic waves by sources located in magnetoactive plasma were investigated.[1-5] The power supplied to the source (electric or magnetic antenna) was often sufficient to influence the plasma around it and to give rise to nonlinear effects during the propagation of the emitted waves. This has acted as a stimulus to studies of nonlinear problems in the interaction between radiation and plasma, taking into account the specific boundary conditions on the source.[6-8] On the other hand, even when the power level is relatively low, there is the question of the energy distribution in the wave spectrum radiated by the source and, above all, the problem of the electromagnetic and electrostatic mode excitation coefficients (MECs). The propagation conditions for these two modes are very different. There is particular interest in this connection in the frequency range ($\Omega_{lh} < \omega \ll \omega_{He} \ll \omega_{pe}$), where Ω_{lh} is the lower hybrid frequency and ω_{pe} and ω_{He} are the plasma and gyro frequencies of electrons. This frequency range is characterized by the presence (in cold homogeneous plasma) of two types of extraordinary wave, namely, the whistler mode with refractive index $n_2^c = \omega_p^2/\omega\omega_{He}|\cos\theta|$, where θ is the angle between the wave vector **k** and magnetic field H_0, and the electrostatic wave, determined by the dispersion relation $\tan\theta = \omega_{He}/\omega$. The excitation of these modes will be discussed below.

Estimates show that, in general, the MECs are very different[9] and depend significantly on the parameters of the ambient medium. This is due not only to the differences between field structures and dispersion properties of radiated waves, but also the redistribution of the near-field of the source in plasma. The point is that a self-consistent distribution of electric field and charged-particle density is formed in the plasma in the neighborhood of the antenna, which interacts with the surface of the antenna[10] and determines the "effective" characteristics of the source, i.e., the magnitude and distribution of the extraneous current and, consequently, the electric and magnetic moments of the source.

Particle settling processes have the most significant effect at low frequencies ($\omega \ll \omega_{pe}$), when the self-consistent distribution of the near field can "follow" the high-frequency field. These processes are also found to lead to a class of nonlinear phenomena due to the nonlinear dependence of the antenna current I and surface charge Q on the magnitude of the applied voltage U, including the excitation of current harmonics, the dependence of antenna matching to the plasma on the amplitude of the applied voltage, and so on. When compared with effects due to the self-interaction of waves, these phenomena become manifest for lower values of the high-frequency power supplied to the source.

Studies of MECs are complicated still further by the presence of intrinsic or radiation-induced plasma inhomogeneities. Our aim in the investigation reported here was to carry out an experimental study of the above problems for a magnetic source. This involved simultaneous measurements of source field and impedance, and a detailed theoretical analysis of the radiated-field structure in a weakly inhomogeneous magnetoactive plasma.

1. EXPERIMENTAL RESULTS

1. The experiments were performed in a vacuum chamber 150 cm long and 80 cm in diameter. The gas was ionized by inducing a discharge in helium at a pressure of about 0.01 torr in a uniform magnetic field of about 400 Oe. The measurements were carried out immediately after the ionizing source was removed, i.e., in decaying plasma (characteristic decay time $\tau = 1$ ms), in which the electron density N_e was between $\sim 10^{13}$ and $\sim 10^{10}$ cm^{-3} (Fig. 1a). The corresponding electron temperature was $T_e \simeq 1$ eV and was equal to the ion temperature.

The antenna (a current-carrying loop) had a diameter of 5 cm and was placed on the axis of the plasma column (diameter typically 40 cm) at right angles to the magnetic lines of force. The antenna was connected to a freely running high-frequency generator producing a maximum output-voltage amplitude of 5 V across a matched load. The working frequency range 20–60 MHz was chosen so that $\Omega_{lh} < \omega \ll \omega_{He}$ ($\Omega_{lh} \simeq 8 \times 10^7$ s^{-1}, $\omega_{He} \simeq 8 \times 10^9$ s^{-1}). The frequency ω was large in comparison with the effective electron collision frequency $\nu_{eff} \simeq 2 \times 10^7$ s^{-1}.

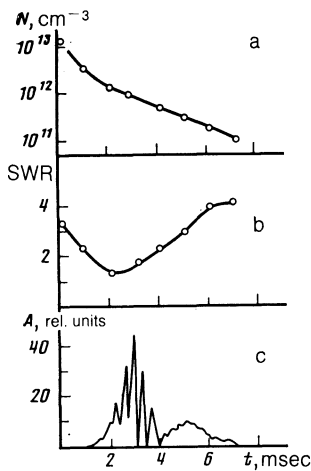The SWR and the impedance of the radiating antenna

FIG. 1. Electron density (a), SWR of the radiating antenna (b), and oscillogram of the signal from the receiving antenna (c) on the axis of the system ($z = 50$ cm from the source).

FIG. 2. Real (O) and imaginary (●) parts of the antenna impedance as functions of density.

were measured with a coaxial directional coupler and a Rogowski loop placed on one of the antenna inputs. The electromagnetic field in the plasma was recorded by frame antennas, 10 mm in diameter and 1 mm thick, which could be displaced to any point in the vacuum chamber. The dispersion properties of waves excited in the plasma were investigated by the phase method.

2. The impedance and the SWRs of the antenna system were investigated in detail in the course of the experiment as functions of frequency and amplitude of the input signal for different values of the plasma parameters. Below, we briefly consider the results of these investigations, at least to the extent to which this will be necessary for an understanding of antenna radiation problems.

Measurements of the impedance and the SWRs showed that there was a definite plasma electron density N_s for which the antenna was fully matched (SWR $\simeq 1.3$) to the high-frequency generator (Fig. 1b). A significant rise in the amplitude of the high-frequency signal in the plasma was recorded when this matching was achieved (Fig. 1c). It was found that, at the instant of matching, the imaginary part of the impedance was close to zero and the real part was 40–60 Ω, i.e., it was close to the internal resistance of the generator (Fig. 2). The electron density N_s was found to be a function of the frequency and amplitude of the signal received by the antenna. As the frequency was reduced, or signal amplitude increased, the matching point was found to shift toward denser plasma.

Figure 3 shows the equivalent circuit of the magnetic antenna in plasma, and constitutes a generalization of the experimental data. It is a parallel resonant circuit in which R_g and C_g are, respectively, the resistance and capacitance of the double layer, R_Σ^M is the radiation resistance of the magnetic dipole, and $|Z_{pl}|$ is the capacitance of the loop (due to its nonideal character) in inhomogeneous plasma. We shall not analyze in detail the parameters R_g and C_g that relate the current I_ω and charge Q_ω of the settling particles to the voltage U_ω at frequency ω, and will confine ourselves to noting that estimates indicate that $|Z_{pl}| \gg C_g$, so that the resonance properties of the circuit are determined by the impedance of the double layer (the inductance of the loop in magnetized plasma is close to its vacuum value[11] L_A). For a
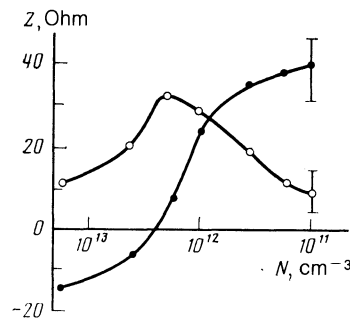
certain value r_{De} (N_s), i.e., at the matching point, the reactance of the circuit falls to zero, the current in the circuit increases, and the result is an increase in the radiated energy.

3. Let us now consider the results obtained by investigating the structure of the electromagnetic field produced by the antenna in plasma. Figure 1c shows a typical signal oscillogram from the receiving antenna, illustrating the time dependence of the magnetic-field amplitude (in this case, the H_z component at a given point). An appreciable signal is recorded by the antenna at the matching time t_s and at subsequent times at which the impedance of the source becomes inductive. As a rule, the oscillogram has two maxima separated by $T \simeq 2$ ms. The first of these has a large amplitude, but the relative amplitude decreases with increasing distance from the radiating antenna, and practically vanishes at the distance $z \simeq 100$ cm. The particular feature of this signal is its fine structure, i.e., the deep amplitude modulation of the first maximum. The modulation time τ_M varies between 300 and 500 μs, depending on the plasma density and the position of the receiving antenna.

This modulation was not observed for the second maximum. Amplitude measurements showed that the field was concentrated near the axis of the system, although its structure depended significantly on the plasma particle density. Phase measurements enabled us to establish that a wave with a constant wavelength $\lambda \simeq 15$–30 cm was propagating along the axis of the system for $t \gtrsim t_s$, which corresponded to a longitudinal wave number $k_z \simeq 0.4$–0.2 cm^{-1}. This enabled us to plot graphs of $k_z(\omega)$ and $k_z(\omega_{He})$, which characterized the dispersion properties of the waves.

2. THEORETICAL MODEL

1. The field structure and the mode excitation coefficients of the magnetic antenna for whistler-mode and electrostatic waves were calculated for our experimental conditions and the results were compared with experimental data.
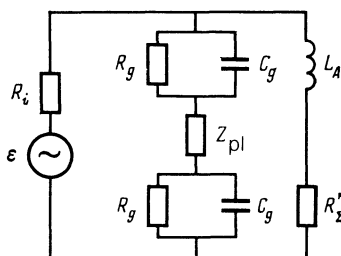
We assumed that the plasma was homogeneous along

FIG. 3. Equivalent circuit of the magnetic antenna in plasma.

the external magnetic field, but that its density in the transverse plane was given by $N_e(r) = N_0 \exp(-ar^2)$. Suppose that the extraneous current has the axisymmetric distribution $j(r,z)\exp(-i\omega t)$ which oscillates with frequency ω. Taking the Fourier transform with respect to z, and using the Maxwell equations, we obtain the following set of equations for field components the E_z and H_r in cold magnetoactive plasma:

$$\frac{1}{r}\frac{\partial}{\partial r}\left(r\frac{\varepsilon_1}{k_1^2}\frac{\partial E_z}{\partial r}\right) - \varepsilon_3 E_z + \frac{k_0}{r}\frac{\partial}{\partial r}\left(\frac{g}{k_1^2}rH_r\right) \qquad (1)$$

$$= \frac{4\pi}{ck_0}\left(ij_z + \frac{k_z}{r}\frac{\partial}{\partial r}\frac{r}{k_1^2}j_r\right),$$

$$\left\{\Delta_\perp - \frac{1}{r^2} + \left(\frac{g^2k_0^4}{k_1^2} - k_1^2\right)\right\}H_r + \frac{k_0gk_z^2}{k_1^2}\frac{\partial E_z}{\partial r}$$

$$= \frac{4\pi k_z}{c}\left(ij_\varphi - \frac{gk_0^2}{k_1^2}j_r\right), \qquad (2)$$

where $k_1^2 = k_z^2 - k_0^2\varepsilon_1$, $k_0 = \omega/c$, and ε_1, ε_3, and g are the components of the permittivity tensor of the cold plasma $(\varepsilon_{xx} = \varepsilon_{yy} \equiv \varepsilon_1, \varepsilon_{zz} = \varepsilon_3, \varepsilon_{xy} = -\varepsilon_{yx} = ig)$.

For a homogeneous plasma, Eqs. (1)–(2) lead to the well-known dispersion relation[12] which, in the frequency range in which we are interested $(\Omega_{\mathrm{lh}} \ll \omega \ll \omega_{He} \ll \omega_{pe})$, and if the condition $k_z \gg 2k_0\varepsilon_1^{1/2}$ is satisfied, takes the form

$$(k_\perp^2 - \varkappa_1^2)(k_\perp^2 - \varkappa_2^2) = 0, \qquad (3)$$

where $\varkappa_1^2 = -(\varepsilon_3/\varepsilon_1)k_z^2 + 2\varepsilon_3k_0^2$ corresponds to electrostatic waves and $\varkappa_2^2 = -k_z^2 + g^2k_0^4/k_z^2$ to whistler modes.

It is clear that $\varkappa_1 \gg \varkappa_2$, i.e., the lateral mode scales are very different. This enabled us to transform without difficulty from (1), (2) to the equations describing each of the modes. The range of wave numbers $k_z \gtrsim 2k_0\varepsilon_1^{1/2}$ requires a more complicated description, but we shall assume that most of the energy is radiated for $k_z \gg 2k_0\varepsilon_1^{1/2}$.

We shall take the source to be a thin frame of radius a, whose plane is perpendicular to the magnetic field. The condition $\alpha = 2.5\ \mathrm{cm} \ll a^{-1} = 20\ \mathrm{cm}$ was well satisfied in our experiment. We shall see that the wave field of this source is confined to the axis of the system, so that the function $N_e(r)$ can be approximated by a parabola throughout the range, and can be taken from under the derivative sign when differentiation with respect of r is carried out in (1) and (2).

2. Let us begin by considering the generation of electrostatic waves. The term $\varkappa_2^2 H_r$ can then be neglected in (2). Applying the operator $\Delta_\perp$ to (1), and substituting the expression for $(\Delta_\perp - 1/r^2)H_r$ in terms of E_z and j_φ, we obtain the following equation for E_z from the second equation $(j_r = j_z = 0)$:

$$\Delta_\perp(\Delta_\perp + \varkappa_1^2)E_z = -\frac{4\pi i\omega}{c^2}k_z\frac{g}{\varepsilon_1}\frac{1}{r}\frac{\partial}{\partial r}rj_\varphi. \qquad (4)$$

To lowest order in $\varepsilon_1 k_0^2/k_z^2$, the term $\varkappa_1^2$ does not depend on the electron density, i.e., $\varkappa_1^2 \simeq \omega_{He}^2 k_z^2/\omega^2$. Consequently, so long as $\omega_{pe} \gg \omega_{He}$, the inhomogeneity has no effect on the electrostatic-wave propagation. Hence, Eq. (4) can be solved by the Fourier method, and the correction $\varkappa_1^2$ arising because the electrostatic waves are not curlfree can be written in the form $2\varepsilon_3 k_0^2 \simeq -2\omega_{pe}^2(0)/c^2$. If, in addition, we

take into account the dissipative correction due to collisions between electrons and ions or neutrals (collision frequency $\nu = \nu_{\mathrm{eff}} \ll \omega$), we can write the solution of (4) in the form $(z > 0)$

$$E_z = \frac{ik_0I_{\mathrm{eff}}}{\omega_{He}}$$

$$\cdot \int_0^\infty \exp\left[i\varkappa z\left(\mu + \frac{k_c^2}{\varkappa^2} + i\frac{\nu}{\omega_{He}}\right)\right]J_0(\varkappa r)J_1(\varkappa a)\,d\varkappa, \qquad (5)$$

where $I_{\mathrm{eff}} = 2\pi ak_0I$, $k_c^2 = k_0^2g_0$, $\mu = \omega_{He}$, and I is the current amplitude in the frame. The other field components can be written in a similar way. We shall now examine in greater detail the expressions for the component H_z measured in the experiment:

$$H_z = \frac{k_c^2I_{\mathrm{eff}}}{\omega}$$

$$\cdot \int_0^\infty \exp\left\{i\varkappa z\left(\mu + \frac{k_c^2}{\varkappa^2} + i\frac{\nu}{\omega_{He}}\right)\right\}J_0(\varkappa r)J_1(\varkappa a)\varkappa^{-1}\,d\varkappa. \qquad (6)$$

It follows from (5) and (6) that the field in the electrostatic wave packet has a maximum for $r^2 - (\mu z - a)^2 < 0$, bounded by conical resonance surfaces. In the collisionless limit, the electrostatic field due to the frame has a singularity on these surfaces.

The particular feature of this problem is that the electrostatic waves propagate almost along the magnetic field (at an angle $\mu \ll 1$), so that, at elevated plasma densities $(N_e \gtrsim 10^{11}\ \mathrm{cm}^{-3})$, the distance between the plane of the frame and the focal point $z_f = a/\mu$ is greater than the wavelength $2\pi/k_c\mu^{1/2}$ of the electromagnetic wave, formed (at large distances from the source) near the resonance cone (see Ref. 13 for further details). The result is that the electrostatic wave packet excited by the frame is found to be amplitude-modulated. This can be verified by deriving the explicit expression for the magnetic field of the packet at $r = 0$, i.e., on the axis of the system:

$$H_z = \frac{2k_c^2I_{\mathrm{eff}}}{\omega}J_1\{\gamma^{1/2}[(b^2+a^2)^{1/2}-b]^{1/2}\}K_1\{\gamma^{1/2}[(b^2+a^2)^{1/2}+b]^{1/2}\} \qquad (7)$$

where $\gamma = -i2k_c^2z$, $b = (\nu/\omega_{He} - i\mu)z$, and J_1 and K_1 are the Bessel functions of the first and second kinds of order 1. Near the focus $z = z_f$, the expression given by (7) has the following form when collisions are neglected:

$$H_z = -\frac{k_c^2I_{\mathrm{eff}}}{\omega}\pi J_1((2\mu)^{1/2}k_cz)H_1^{(1)}((2\mu)^{1/2}k_cz), \qquad (8)$$

where $H_1^{(1)}$ is the Hankel function. The presence of the factor $J_1((2\mu)^{1/2}k_cz)$ shows that the wave packet amplitude is modulated in space with a characteristic longitudinal scale $z_{\mathrm{M}} \simeq (2\pi/k_c)(2\mu)^{1/2}$. Since the experiments were carried out in decaying plasma, in which the electron density varied in accordance with the expression $N_e(t) = N_0\exp(-t/\tau)$ with a characteristic time $\tau \sim 1\ \mathrm{ms}$, the signal produced by the receiving antenna at a given point z was proportional to

$|H_z|^2$, and could be amplitude-modulated in time. The characteristic modulation time can be estimated from the formula

$$\tau_{\text{M}} = \tau \pi c / 2^{1/2} \mu z \omega_{pe}. \tag{9}$$

For $z = z_f = 85$ cm and $N_e = 10^{12}$ cm^{-3}, this gives $\tau_{\text{M}} = 0.45$ ms.

It follows from (7) that the effects of collisional dissipation are significant for $z \gtrsim a/(\nu/\omega_{He})$, i.e., they have very little effect on the field structure for $\nu < \omega$ and distances $z < z_f$. If, at the same time, at long wavelengths ($k_c \ll \mu^{1/2}/a$), electromagnetic effects are not significant at distances less than the focal length and the amplitude of the field is constant, i.e., $|H_z| = k_c^2 I_{\text{eff}}/\omega$. In the opposite limit ($k_s \gg \mu^{1/2}/a$), expression (7) has the following form for distances $(2k_c^2 a)^{-1} \ll z \ll a/\mu$:

$$H_z = -\frac{k_c I_{\text{eff}}}{\omega (2az)^{1/2}} \{\exp[-2k_c(az)^{1/2}] + i \exp[2ik_c(az)^{1/2}]\}. \tag{7'}$$

Consequently, the magnetic-field amplitude is proportional to $z^{-1/2}$. However, formula (8) shows that, in the neighborhood of the focus, $|H_z|$ increases again, reaching the value $k_c(2\mu)^{1/2} I_{\text{eff}}/\omega a$.

The energy lost by the antenna by the emission of electrostatic waves can be found by evaluating the flux of the quasielectrostatic Poynting vector over a surface surrounding the source. For the above frame, this leads to the following expression for the energy lost per unit time:

$$W_e = 8\pi a^3 \omega^3 g_0 I^2/3c^4. \tag{10}$$

3. Let us now examine the generation of whistler waves. Assuming that the transverse scale β^{-1} of the wave perturbations is large in comparison with $(\omega/\omega_{He})k_z^{-1}$, we can use (1) to express E_z in terms of H_r:

$$E_z = \frac{k_0}{\varepsilon_3 k_z^2 r} \frac{\partial}{\partial r} (rgH_r).$$

Substituting this expression in (2), we can then verify that the term proportional to $\partial E_z/\partial r$ is a small correction (in the parameter $k_0^2 \varepsilon_1/k_z^2$) to the term $(\Delta_\perp - 1/r^2)H_r$. The equation describing the emission of whistler waves therefore has the form

$$\Delta_\perp H_r - \frac{H_r}{r^2} + \left(\frac{g^2 k_0^4}{k_z^2} - k_z^2\right)H_r = \frac{4\pi i k_z}{c} j_\varphi. \tag{11}$$

Since $N_e(r) = N_0(1 - \alpha^2 r^2)$, the corresponding homogeneous equation takes the form

$$\frac{1}{r}\frac{\partial}{\partial r}\left(r\frac{\partial H_r}{\partial r}\right) - \frac{H_r}{r^2} + \left\{\left(\frac{k_0^4 g_0^2}{k_z^2} - k_z^2\right) - 2\frac{k_0^4 g_0^2}{k_z^2}\alpha^2 r^2\right\}H_r = 0. \tag{12}$$

Although the density gradient is assumed weak ($k_z \gg \alpha$), it plays a fundamental part in this case, since it determines the discrete spectrum of the whistler waves. To show this, we seek the solution of (12) in the form

$$H_r = \xi^{1/2} e^{-\xi/2} w(\xi), \quad \xi = \frac{2^{1/2}\alpha k_0^2 g_0}{k_z} r^2. \tag{13}$$

The function $w(\xi)$ satisfies the equation

$$\xi w'' + (2-\xi)w' + nw = 0, \tag{14}$$

where

$$n = \left(\frac{k_0^4 g_0^2}{k_z^2} - k_z^2\right)\left(\frac{4 \cdot 2^{1/2}\alpha k_0^2 g_0}{k_z}\right)^{-1} - 1.$$

Solutions of (14) that are bounded and decrease satisfactorily at infinity exist only for values of n that are nonnegative integers. They take the form of the confluent hypergeometric functions[14] $w = F(-n,2;\xi)$. The dispersion relation describing the spectrum of longitudinal wave numbers must therefore have the form

$$\frac{k_0^4 g_0^2}{k_z^2} - k_z^2 = 4 \cdot 2^{1/2} \frac{\alpha k_0^2 g_0}{k_z}(n+1), \tag{15}$$

where $n = 0,1,2,\ldots$. When $k_z \gg \alpha$, the solution is given by the elementary expression

$$(k_z)_n = k_0 g_0^{1/2} - 2^{1/2}\alpha(n+1). \tag{16}$$

This solution is valid when the correction to $k_z g_0^{1/2}$ is small.

When n is an integer, the function $F(-n,2;\xi)$ is a polynomial of degree $2n$:

$$F(-n, 2; \xi) = (n+1)^{-1}L_n^1(\xi),$$

where L_n^1 is the Laguerre polynomial. The eigenfunctions corresponding to zero and first modes are

$$(H_r)_0 = re^{-\beta_0^2 r^2}; \quad (H_r)_1 = r(1-\beta_1^2 r^2)e^{-\beta_1^2 r^2}, \tag{17}$$

where $\beta_n^2 = \alpha k_0^2 g_0/2^{1/2}k_{zn}$. The other field components can be expressed in terms of H_r as follows:

$$H_\varphi = g_0^{1/2} E_r = -iH_r, \quad E_\varphi = -g_0^{-1/2} H_r,$$

$$H_z = -g_0^{1/2}\mu^{-1}E_z = k_0^{-1}g_0^{-1/2}\frac{1}{r}\frac{\partial}{\partial r}rH_r. \tag{18}$$

It follows from these that the whistler field components obey the following inequality:

$$|H_r| \approx |H_\varphi| \gg |E_r| \approx |E_\varphi| \gg |E_z|, \quad |H_r| \gg |H_z| \gg |E_z|,$$

$$|H_z|/|E_\varphi| \approx (\alpha g_0^{1/2}/k_0)^{1/2}.$$

In our experiments, $|H_z| > |E_\varphi|$.

Since the set of eigenfunctions $\mathbf{H}_n$, $\mathbf{E}_n$ is complete, the electromagnetic field of the source can be expanded in the form

$$\mathbf{H} = \sum_{n=0}^{\infty} A_n \mathbf{H}_n, \quad \mathbf{E} = \sum_{n=0}^{\infty} A_n \mathbf{E}_n.$$

The coefficients A_n can be found with the aid of the complex Lorentz Lemma:

$$4A_n\Pi_n = A_n \cdot 2c \int_0^\infty |H_{rn}|^2 r\, dr = \int \mathbf{j}\mathbf{E}_n\, d\mathbf{r}, \tag{19}$$

where the integral on the right is evaluated over the region occupied by the extraneous current inside the waveguide and Π_n is the energy flux transported by the nth mode of unit amplitude ($A_n = 1$).

The coefficient of excitation of the nth mode by the ex-

traneous source, i.e., the energy lost by the source per unit time by the emission of the nth mode is obviously given by $W_n = |C_n|^2 \Pi_2$, so that, if we use (13) and (19), we find that, for the above frame,

$$W_n = \frac{4\pi^2 I^2 a^4 \beta_n^4}{cg_0^{1/2}} e^{-2\beta_n^2 a^2} \{F(-n, 2; 2\beta_n^2 a^2)\}^2 (n+1). \quad (20)$$

It follows from this that the excitation coefficient W_n is determined by the parameter $A^2 \beta_n^2$, i.e., the ratio of the radius of the frame to the lateral scale of the whistler field.

For $k_0 g_0^{1/2} > > > \alpha$, the spectrum of wave numbers k_{zn} is quasiperiodic, and the sources excites many modes, i.e., we have a transition to the homogeneous medium. In point of fact, the total energy lost (per unit time) by the source as a result of the emission of whistler waves is

$$W_c = \sum_n W_n.$$

The condition $\Delta k_z = 2^{1/2} \alpha \ll k_0 g^{1/2} - 2\varepsilon_1^{1/2}$ enables us to transform from summation over n to integration over k_z. Since in a homogeneous plasma the wave with $k_z < 2k_z \varepsilon_1^{1/2}$ does not propagate, it is natural to take $k_{zp} = 2k_0 \varepsilon_1^{1/2}$ as the lower limit for the range of integration. Assuming that $\alpha k_0 \alpha^2 \ll 2 \times 2^{1/2} \mu^{1/2}$, we find that

$$W_c = \frac{\pi^2 I^2 a^4 k_0^4 g_0^{1/2}}{c} \left\{ \frac{1}{2} \mu^{-1/2} - \left[1 + \ln\left(\frac{1}{2} \mu^{-1/2} \right) \right] \right\}. \quad (21)$$

The result is thus seen to be independent of a, and the ratio W_c/W_0 is determined by the parameter $k_0^2 g_0/\alpha^2 \gg 1$. If we compare W_c with the intensity of the electrostatic waves, we obtain

$$\frac{W_c}{W_e} = \frac{3\pi}{8} \alpha k_0 g_0^{1/2} \left\{ \frac{1}{2} \mu^{-1/2} - \left[1 + \ln\left(\frac{1}{2} \mu^{1/2} \right) \right] \right\}. \quad (22)$$

The formulas given by (21) and (22) were used in the experiment, but only for very high values of electron density $(N_e > 10^{12}$ cm$^{-3})$. For example, for $N_e = 4 \times 10^{12}$ cm^{-3} (six modes excited), the above estimates give $W_c/W_e \simeq 1.4$. The ratio W_c/W_e decreases with decreasing N_e, but the width of the transparency interval, $k_0 (g_0^{1/2} - 2\varepsilon_1^{1/2})$, becomes comparable in order of magnitude with the "mode separation" $\Delta k_z = 2^{1/2} \alpha$, and (22) is invalid. Only the fundamental whistler mode propagates when $N_0 < 4 \times 10^{11}$.

The coefficient of excitation of the zeroth mode, divided by the electrostatic-wave power is given by

$$\frac{W_0}{W_e} = \frac{3\pi (a\beta_0)^4}{2 (ak_0 g_0^{1/2})^3} e^{-2(\beta_0 a)^2}, \quad \beta_0^2 = \frac{\alpha k_0^2 g_0}{2^{1/2} k_{z0}}. \quad (23)$$

When $N_e \simeq 5 \times 10^{11}$ cm^{-3}, we have $W_0/W_e \simeq 0.18$. The ratio W_0/W_e increases somewhat with decreasing N_e, but we find that $k_{z0} \simeq 2k_0^2 \varepsilon_1^{1/2}$ when $N_e \simeq 10^{11}$ cm^{-3}, and the wave guide becomes opaque to whistler waves. It can be shown that the collisional attenuation of the whistler waves for $k_{zn} \gg \alpha$ is equal to the attenuation of a monochromatic whistler mode propagating along the field: $\mathrm{Im} k_{zn} \simeq (\nu/2\omega_{He}) k_{zn}$. On the other hand, estimates show that the linear transformation of the zeroth mode into electrostatic waves for $\omega \ll \omega_{He}$ is exponentially small because of the considerable difference between the spatial scales of the corresponding waves along and at right angles to the magnetic field.
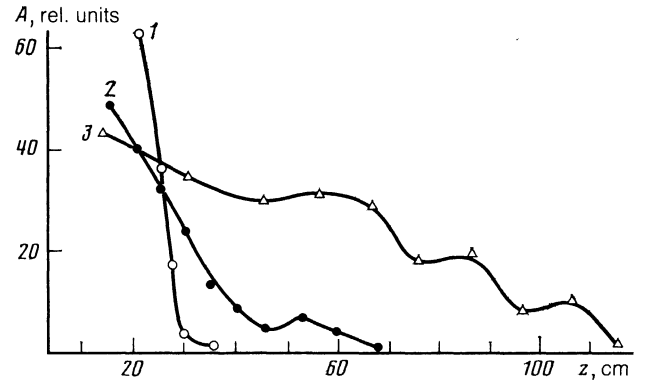

FIG. 4. Amplitude of the field H_z on the axis of the system for different values of the plasma density: 1—$N_e = 3 \times 10^{12}$ cm^{-3}, 2—$N_e = 1.8 \times 10^{12}$ cm^{-3}, 3—$N_e = 6 \times 10^{11}$ cm^{-3}.

Thus, the spatial damping rate of the zeroth mode was negligible in the experiments that we are considering here.

3. DISCUSSION OF EXPERIMENTAL RESULTS

Comparison of calculations with experimental data shows that, as the charged-particle density is varied in the chosen range, the properties of the radiating antenna undergo a significant change. When $N_e < N_s$, the experimental results can be explained in terms of the above analysis of the radiation field due to a current-carrying loop. For $N_e > N_s$ (in which case the reactance of the antenna is capacitive), an adequate description of the frame antenna must involve both magnetic and electric sources, where the latter intensively excite electrostatic waves with a characteristic lateral scale L_e of the order of the wire diameter, i.e., $\ll a$. In point of fact, the field rapidly decreases with distance from the source for large N_e (curve 1, Fig. 4), which shows that the emission spectrum is dominated by small-scale electrostatic waves. Analysis of the lateral field structure near the antenna then determines the increase in the field in the region of the resonance cone (Fig. 5).

For $N_e < N_s$, the effective electric moment of the frame is reduced, and it may be looked upon as a magnetic source. According to the foregoing estimates, much of the radiated energy is then again carried by the electrostatic waves, but the characteristic scale is greater, i.e., $L_e \simeq a$. Moreover, as the collision frequency ν_{eff} decreases, this leads to the "stretching" of the field along the axis of the system (curves 2 and 3 of Fig. 4). At the same time, the current-carrying loop efficiently excites the whistler waves. When $N_e \lesssim 6 \times 10^{11}$ cm^{-3}, so that the zeroth mode appears in the spatial spectrum of the whistler waves, phase measurements show the presence near the axis of the system of a propagating wave whose longitudinal scale is the perfectly definite
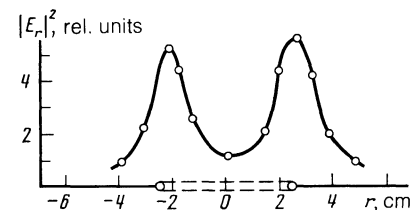

FIG. 5. Lateral distribution of the electric field ($|E_r|^2$) near the radiating antenna ($z \gg 1$ cm).

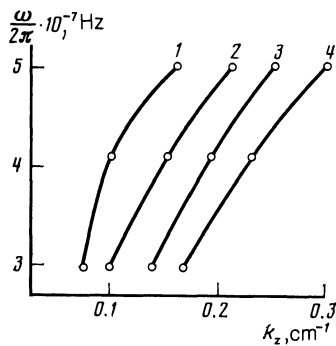FIG. 6. Dispersion curves calculated from phase measurements: 1—$N_e = 2.4 \times 10^{11}$ cm^{-3}, 2—$N_e = 3.6 \times 10^{11}$ cm^{-3}, 3—$N_e = 4.7 \times 10^{11}$ cm^{-3}, 4—$N_e = 6 \times 10^{11}$ cm^{-3}.

FIG. 8. Lateral distribution of the electric-field amplitude: a—$N_e = 1.1 \times 10^{12}$ cm^{-3}, b—$N_e = 6.5 \times 10^{11}$ cm^{-3}.

quantity λ_z that varies (depending on N_e) in the range 17–30 cm. The measured wavelength and also the dispersion curves $\omega(k_z)$ (Fig. 6) obtained for different values of the electron density are in good agreement with the dispersion relation for the zeroth mode: $k_{z0} = k_0 g_0^{1/2} - 2^{1/2} \alpha$. Estimates of the transverse scale of the field distribution in the zeroth mode give

$$\beta_0^{-1} = (2^{1/2} k_0 g_0^{1/2} \alpha^{-1} - 2)^{1/2} (k_0 g_0^{1/2})^{-1} \approx 9 \text{ cm}$$

for $N_e = 5 \times 10^{11}$ cm^{-3}, which again is in agreement with experimental results (Fig. 7). According to (23), a reduction in density leads to an increase in the ratio W_0/W_e, but, for $N_e \simeq 2 \times 10^{11}$ cm^{-3}, the radiation field becomes very weak because the antenna is no longer in the matched state.

The oscillogram of the signal amplitude recorded by the receiving antenna (Fig. 1c) at a fixed point near the axis of the system illustrates the above changes in the working of the radiation source. As noted before, these oscillograms are typically highly modulated. In accordance with the above calculations, this modulation is an indication that an electrostatic wave packet is being excited. The modulation period is in agreement with calculations, and increases as the plasma decays, in accordance with (9). Naturally, the time-domain amplitude modulation is related to the amplitude modulation in space (Fig. 8). As the plasma decays, the space distribution stretches out, so that the corresponding maxima and minima of the field amplitude cross the given points, and we observe the modulation on the oscillograms. For sufficiently
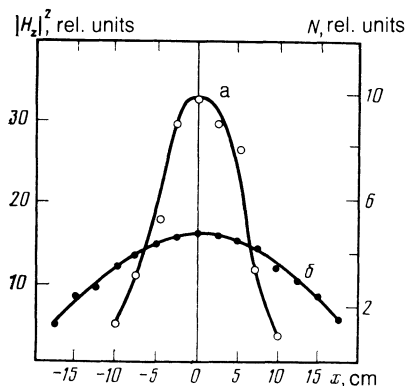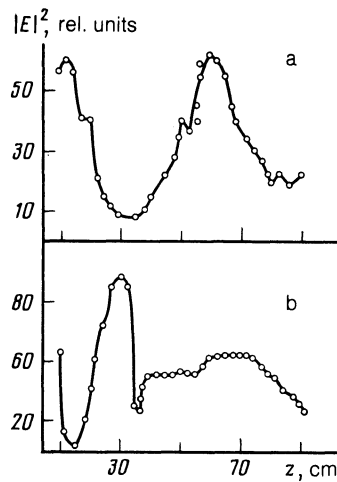
small $N_e = N_{ep}$, the amplitude distribution minimum nearest to the plane of the loop crosses the point of observation, but there is no modulation for smaller N_e. For example, if the point of observation lies near the focus, the approximate formula $N_{ep} = (2 \times 2^{1/2} \quad c/5.6 \times 10^4 \quad \mu z)^2$ gives $N_{ep} \simeq 5 \times 10^{11}$ cm^{-3}, which is close to the experimental result.

We emphasize that the longitudinal field-amplitude distributions shown in Fig. 4 were obtained from the envelope of the signal amplitude recorded by the receiving antenna, and do not therefore reflect the presence of the spatial modulation of the amplitude of the electrostatic wave packet which, in contrast to the curves of Fig. 8, gives the instantaneous distribution of the field amplitude (and not the distribution averaged over the modulation period τ_M).

Since for $N_e \lesssim 6 \times 10^{11}$ cm^{-3} the frame may be looked upon as a magnetic source, and most of the energy radiated by it is expended in exciting electrostatic waves, the radiation resistance of the frame can be estimated from (10):

$$R_s = 2W_e/I^2 = 16\pi a^3 \omega^3 g_0/3c^4.$$

For $N_e = 4 \times 10^{11}$ cm^{-3}, we have $R_s = 2\Omega$. On the other hand, when the reactance of the antenna is inductive, the equivalent circuit of Fig. 3 enables us to determine the radiation resistance from measured values of ReZ and ImZ. When $N_e = 4 \times 10^{11}$ cm^{-3}, we have $R_s \simeq 1.3\Omega$, which is of the order of the theoretical estimate.

CONCLUSIONS

Our investigations have enabled us to establish the properties of the magnetic antenna in the lower hybrid frequency range, and to put forward relatively simple models for them. Without recapitulating all the results, we emphasize only two:

1. We have established that settling of charged particles can play a fundamental part in the lower hybrid frequency range, since it determines the impedance of the antenna in plasma. A substantial proportion of the energy fed into the antenna is expended in heating the particles in the double layer; in our experiments, this energy exceeded the radiative energy loss (per unit time) by at least an order of magnitude.

2. Simultaneous measurements of field and impedance,

FIG. 7. Lateral distributions: a—field H_z, b—plasma with $N_{e0} = 10^{12}$ cm^{-3} ($z = 90$ cm).

taking into account detailed calculations of the field structure, enabled us to identify the modes radiated by the source for different charged-particle densities in the plasma and, in some cases, to measure the SWR and to compare the results with calculations. The satisfactory agreement between theory and experiment, including relatively delicate effects and estimates (modulation of the electrostatic wave packet, identification of the zeroth mode in the whistler spectrum, and estimates of the radiation resistance of the antenna) indicate that the theoretical models are essentially correct. Our results can therefore be used to interpret and forecast the data of both laboratory and space experiments. In particular, they enable us to calculate the mode excitation coefficients of electrostatic and whistler waves for given plasma parameters (unperturbed plasma or plasma modified by the electromagnetic field) near the antenna.

The authors are indebted to A. V. Kudrin and V. A. Mironov for useful discussions.

[1]*Active experiments in space*, Proc. of an Int. Symposium at Alpbach, Austria, in 1983, p. 375.

[2]Yu. I. Gal'perin, R. Z. Saydeev, F. K. Shuyskaya *et al.*, Kosm. Issled. **19**, 34 (1981).

[3]H. Sugai, H. Niki, S. Takeda and M. Inutake, Phys. Fluids **23**, 2134 (1980).

[4]H. C. Koons, D. C. Pridmore–Brown, and D. A. McPherson, Radio Sci. **9**, 541 (1974).

[5]G. You. Golubyatnikov, S. V. Egorov, and A. V. Kostrov *et al.*, Int. Conf. on Plasma Physics, Kiev, **4**, 145 (1987).

[6]N. S. Erokhin, M. V. Kuzelev, S. S. Moiseev *et al.*, Nonequilibrium and Resonance Procession in Plasma Radiophysics [in Russian], Nauka, Moscow, 1982, p. 106.

[7]W. S. Wang and H. H. Kuehl, Phys. Fluids, **23**, 566 (1980).

[8]V. N. Goldberg, E. A. Mareev, V. A. Ugrinovskiĭ and Yu. V. Chugunov, Zh. Eksp. Teor. Fiz. **90**, 2013 (1986) [Sov. Phys. JETP **63**, 1180 (1986)].

[9]V. P. Dokuchaev, V. V. Tamoikin, and Yu. V. Chugunov, Izv. vuzov. Radiofizika, **19**, 1121 (1976).

[10]Ya. L. Al'pert, A. V. Gurevich, and L. Pitaevskiĭ, Space Physics with Artificial Satellites Consultants Bureau, New York (1965).

[11]T. N. C. Wang, and T. F. Bell, IEEE Trans. Ap. **21**, 745 (1973).

[12]V. L. Ginzburg, Propagation of Electromagnetic Waves in Plasma, North Holland, Amsterdam (1961).

[13]E. A. Mareev and Yu. V. Chugunov, Izv. vuzov. Radiofizika, **30**, 961 (1987).

[14]L. D. Landau and E. M. Lifshitz, *Quantum Mechanics* [in Russian], Nauka, Moscow, 1973, p. 97 [English translation by Pergamon Press, various eds.].

Translated by S. Chomet